

Isolation Performance of Optimized Triple Friction Pendulum

Felix Weber¹, Hans Distl², Christian Braun³

¹(Maurer Switzerland GmbH, Zurich, Switzerland)

²(Maurer Engineering GmbH & Co. KG, Munich, Germany)

³(MAURER SE, 80807 Munich, Germany)

Abstract: This paper compares the isolation performance of the triple friction pendulum (FP) with that of the double FP as benchmark. First, both FPs are optimized for minimum absolute structural acceleration. In order to break down the hardly tractable optimization problem of the triple FP with 12 parameters to a manageable optimization task it is assumed that the effective radii 1 and 4 are given by the targeted isolation time period and the parameters of the articulated slider are selected according to the design philosophy of the triple FP. As a result, the triple FP can be optimized by variation of its friction coefficients 1 and 4 only; the double FP with same isolation time period is optimized by variation of its friction coefficients 1 and 2. Due to the nonlinearity of FPs the optimizations are performed for four accelerograms of real earthquakes in order to take into account the different frequency content of different earthquakes and for three selected PGAs representing smaller, medium and larger DBEs. Subsequent to the optimizations, the optimized FPs are assessed in terms of absolute structural acceleration and total bearing motion for the same earthquakes but scaled to a wide range of PGAs up to the value corresponding to the MCE in order to perform the assessment for all possibly occurring earthquakes. The results reveal that the absolute structural accelerations and total bearing displacements due to the optimized triple and double FPs are very similar within the entire PGA range.

Keywords: Earthquake, isolation, seismic; triple friction pendulum, optimization

I. INTRODUCTION

The base isolation of civil engineering structures is the common countermeasure against hazardous structural vibrations due to earthquake excitation [1-4]. Various types of elastomeric bearings and spherical friction pendulums (FP) belong to the class of passive isolators that exert the superposition of a stiffness force and damping force [5-11]. For minimum structural response the stiffness is designed to significantly increase the fundamental period of the isolated structure with the constraint of the re-centring condition and the friction is tuned to add damping to the structure at isolation frequency [12-15]. Due to the nonlinearity of the friction force the effective damping ratio of the isolator depends on the bearing displacement amplitude [16]. Therefore, the friction coefficient can only be optimized for one selected peak ground acceleration (PGA) value of the earthquake which commonly corresponds to the design basis earthquake (DBE). Consequently, the added damping and the isolation of the structure, respectively, are suboptimal for earthquakes with smaller and larger PGAs. This drawback of conventional FPs may be solved by active, semi-active and hybrid isolation systems based on controlled hydraulic actuators [17], variable orifice dampers [18], variable stiffness devices [19, 20], shape memory alloys [21], electrorheological dampers [22] and magnetorheological dampers [23-25] due to their ability to emulate controllable stiffness and damping forces [26, 27].

The economic disadvantages of these control-based solutions triggered the development of adaptive FPs whose stiffness and friction properties depend on the displacement amplitude at which the FP is operated. Besides double FPs with articulated slider in order to design the double FP with different radii and friction coefficients [28] the triple FP represents a promising solution as these devices exhibit significant adaptability. A detailed description of the working principle, the modelling and testing of triple FPs can be found in, e.g., [29-34]. According to [29] the triple FP is conceptualized to produce low friction combined with high stiffness at small bearing displacements and PGAs, respectively, generate increasing friction combined with softening behaviour at medium to large PGAs due to the DBE and the maximum credible earthquake (MCE), and exhibit stiffening behaviour at bearing displacement amplitudes and PGAs, respectively, resulting from earthquakes beyond the MCE. As a result, the isolation performance of the triple FP has to be assessed for various PGA values in order to ensure that the triple FP is operated within all its sliding regimes with associated equivalent stiffness and damping parameters [35, 36]. These investigations are based on the triple FP as designed in [29] which represents a mock-up FP for laboratory scale experiments which explains the fairly low isolation time period of 1.87 s. In contrast to these investigations the aim of the present paper is:

- a) first, to optimize the triple FP for a selected earthquake scaled to three different PGA values representing a rather small, a medium and a rather large DBE, and

- b) second, to assess the optimized triple FP in terms of absolute structural acceleration (and drift) and total bearing displacement (costs of bearing) within the entire PGA range up to the MCE.

As the structure is simplified by a 1-degree-of-freedom system the drifts are in proportion to the absolute structural accelerations whereby the assessment results of the drifts are omitted. Both the absolute structural accelerations and the total bearing displacements are compared with those obtained from the optimized double FP as benchmark.

The layout of the paper is as follows. First, the optimization procedures of the triple and double FPs based on the targeted isolation time period are described in section 2. The modelling of the structure and the FPs is given in section 3. The optimization results of the triple and double FPs for several ground acceleration time histories that are scaled to three PGA values representing three different DBEs are given in section 4. Section 5 shows and discusses the isolation performance results due to the optimized triple and double FPs for various PGA values ranging from 0.25 m/s^2 up to 150% of the PGA used for optimization in order to assess the FPs also at smaller and larger PGAs than used for optimization. The paper is closed by a summary and conclusions given in section 6.

II. OPTIMIZATION OF TRIPLE FRICTION PENDULUM

The dynamic behaviour of the triple FP is determined by 12 parameters, i.e. four friction coefficients, four effective radii and four displacement capacities of the four sliding surfaces (Fig. 1(a)). Hence, the optimization of the triple FP in general is a hardly tractable optimization problem. In the following it is explained how this complex optimization task can be broken down to a simplified optimization procedure without losing the main features of the triple FP. In the subsequent section it will be shown that the simplified optimization procedure leads to verifiable optimization results as the optimization functions can be displayed by three-dimensional graphs which prove that the global extremum is found by the optimization routine.

2.1 Optimization Criterion

The optimal triple and double FPs are those which minimize the absolute maximum of the absolute acceleration of the structure due to earthquake ground excitation [23]

$$\min \left\{ \max \left(\left| \ddot{u}_s + \ddot{u}_g \right| \right) \right\} \quad (1)$$

where \ddot{u}_s denotes the acceleration of the structure relative to the ground and \ddot{u}_g is the ground acceleration. The structural drift is not considered as additional optimization criterion because absolute structural accelerations are in proportion to structural drifts if the structure is modelled by a single degree-of-freedom system as it is commonly done when the optimization of the isolator is of concern, see e.g. [36].

2.2 Optimization For 12 Different DBEs

The friction and stiffness parameters of the triple FP vary as function of the total bearing displacement due to the different sliding regimes of the triple FP [29, 30, 36]. Hence, both the friction and the stiffness parameters of the triple FP are nonlinear functions of the total bearing motion amplitude whereby also the optimization of the triple FP depends on the bearing displacement amplitude. In order to take into account the displacement dependency of these parameters the triple FP is optimized for minimum absolute acceleration of the building (1) using four different accelerograms that are scaled to three selected PGAs representing three different design basis earthquakes:

- $PGA_{opt} = 2.5 \text{ m/s}^2$ representing a rather small DBE,
- $PGA_{opt} = 5.0 \text{ m/s}^2$ representing a medium DBE, and
- $PGA_{opt} = 7.5 \text{ m/s}^2$ representing a rather large DBE.

Since four earthquakes are considered, i.e. the accelerograms of the measured El Centro North-South (NS), Kobe, Loma Prieta and Northridge earthquakes, that are scaled to three different PGAs, in fact, the optimizations are performed for 12 different DBEs. Hence, the triple FP is not only optimized for different PGAs but also different frequency contents of earthquakes. To ensure comparability, the double FP that also exhibits nonlinear behaviour due to its friction force is optimized for the same four accelerograms that are scaled to the same three values of PGA_{opt} .

2.3 Assessment For All Possible PGAs Of Earthquakes

Once the triple FPs (and double FP as benchmark) are optimized for the selected 12 DBEs the optimized triple FPs are assessed in terms of absolute structural acceleration extreme for the same four earthquakes representing different frequency contents but scaled to various PGAs in order to assess the isolation

performance of the triple FPs that are optimized at one specific PGA (PGA_{opt}) also for the cases that earthquakes with smaller and larger PGAs occur. This is done by scaling the accelerograms of the four selected earthquakes to the PGA values ranging from $0.25 m/s^2$ up to 150% of PGA_{opt} (2). This wide range ensures that the isolation performance (1) is computed for very small but frequently occurring earthquakes far below the DBE, for small to medium earthquakes below and in the vicinity of the DBE and for earthquakes stronger than the DBE. The maximum PGA value considered in this study is selected as 150% of PGA_{opt} which may represent the PGA of the MCE.

$$assessment\ range(PGA): 0.25\ m/s^2, 0.50\ m/s^2, \dots, 1.5\ PGA_{opt} \tag{2}$$

2.4 Isolation Time Period

The isolation time period $T_{isolation}$ is a design parameter of the isolation system. Common practice is to select $T_{isolation}$ between 3 s to 4 s whereby the response of the structure becomes smaller than \ddot{u}_g even without damping in the isolator [16]. In this study $T_{isolation} = 3.5$ s is selected which yields the effective radius R_{eff} of the spherical isolator as follows

$$R_{eff} = g \left(\frac{T_{isolation}}{2\pi} \right)^2 = 3.044m \tag{3}$$

where g denotes the acceleration of gravity. The lower isolation time period of the triple FP is given by the sum of the effective radii R_{eff-1} and R_{eff-4} of sliding surfaces 1 and 4 (Fig. 1(a)). The literature survey on triple FPs shows that $R_{eff-1} = R_{eff-4}$ is adopted which leads to the effective radii 1 and 4 as follows (Table 1)

$$R_{eff-1} = R_{eff-4} = \frac{1}{2} g \left(\frac{T_{isolation}}{2\pi} \right)^2 = 1.522m \tag{4}$$

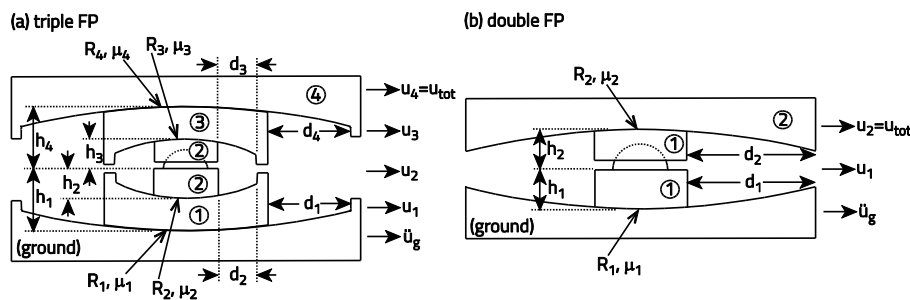


Figure 1. Sketches of triple (a) and double (b) FPs with articulated sliders.

In case of non-adaptive double FPs it is common practice to design both spherical surfaces with the same effective radii, that is (Fig. 1(b))

$$R_{eff-1} = R_{eff-2} = \frac{1}{2} g \left(\frac{T_{isolation}}{2\pi} \right)^2 = 1.522m \tag{5}$$

The geometrical radii follow from the effective radii (4, 5) and the heights h_i according to $R_i = R_{eff-i} + h_i$ (Fig. 1, Table 1).

2.5 Sliding Regime V

The sliding regime V is activated when the restrainers (end stoppers) of sliding surfaces 1 and 4 are triggered whereby sliding only occurs at surfaces 2 and 3 and consequently friction and stiffness of sliding regime V are determined by the low friction and high stiffness properties of surfaces 2 and 3 of the articulated slider assembly of the triple FP [29, 30, 36]. According to the design philosophy of the triple FP given in [29] the aim of sliding regime V is not to generate good isolation of the structure but to limit the required displacement capacity of the triple FP by its stiffening behaviour. As the goal of the optimization procedure here is to minimize the acceleration response of the structure, the sliding regime V is not relevant. Therefore, the triple FP is computed without restrainers 1 and 4 whereby sliding regime V is not triggered at any level of PGA.

As a result, the displacement capacities d_1 and d_4 , respectively, do not require to be specified for the optimization of the triple FP. It should be added that neglecting the end stoppers 1 and 4 will result in slightly better isolation results, i.e. slightly lower structural accelerations, as the stiffening behaviour of sliding regime V is not triggered during the optimization runs. To ensure comparability, the optimization of the double FP is also performed without end stoppers.

2.6 Parameters Of Articulated Slider Assembly Of Triple FP

The intension of the articulated slider assembly is to initiate relative motion between slider and sliding surfaces 2 and 3 at very small PGAs and also if the friction coefficient might be higher during the first couple of cycles due to dry friction effects. The design philosophy is therefore to select small values for the friction coefficients of sliding surfaces 2 and 3. According to the theoretical and experimental results described in [29, 30] the low friction coefficients of sliding surfaces 2 and 3 are selected as follows

$$\mu_2 = \mu_3 = 1.75\% \quad (6)$$

Analogically to the common design approach $R_{eff-1} = R_{eff-4}$ the effective radii R_{eff-2} and R_{eff-3} of the articulated slider assembly are also chosen to be equal, i.e. $R_{eff-2} = R_{eff-3}$, which is in agreement with the design methodology given in the literature. As the aim of the slider assembly is to combine low friction with high stiffness, see [29], the effective radii 2 and 3 are designed far smaller than those of sliding surfaces 1 and 4; in case of the triple FP described in [29] $R_{eff-2} = R_{eff-3}$ are designed to be 8.21 times smaller than $R_{eff-1} = R_{eff-4}$. This design rule is also adopted here which leads to

$$R_{eff-2} = R_{eff-3} = \frac{R_{eff-1}}{8} = 0.190m \quad (7)$$

The displacement capacities d_2 and d_3 of the articulated slider assembly are up-scaled in the same way as the effective radii of sliding surfaces 2 and 3 are greater than those presented in [29]. This proportional up-scaling design yields

$$d_2 = d_3 = 0.07m \quad (8)$$

Notice that d_2 and d_3 hardly influence the optimization results since the restrainers on surfaces 2 and 3 are triggered when the triple FP is operated in sliding regime V and the total displacement capacity is used. However, as restrainers 1 and 4 are omitted for the optimization for the reasons described in section 2.5, also the end stoppers on surfaces 2 and 3 are not activated. Only in case of very high friction coefficients of 15% and higher on surfaces 1 and 4 restrainers 2 and 3 might be triggered. As such high friction coefficients far from being optimal, $d_2 = d_3 = 0.07m$ does not influence the optimal solution.

2.7 Optimization Parameters

The selection of the isolation time period and adopting the common design philosophy for the friction coefficients, effective radii and displacement capacities of the articulated slider assemble of the triple FP, the hardly tractable optimization problem of the triple FP with 12 parameters is broken down a simpler optimization problem with two parameters, i.e. μ_1 and μ_4 . Due to the reduced complexity of the optimization problem it is guaranteed that the globally optimal parameters μ_1 and μ_4 are identified. In addition, the resulting three-dimensional optimization function allows plotting it as a three-dimensional surface showing the sensitivity of μ_1 and μ_4 on the resulting absolute structural acceleration. For the less complex double FP the selection of the isolation time period, which is the same as for the triple FP to ensure fair comparison, yields $R_{eff-1} = R_{eff-2}$ according to (5). As the double FP does not include restrainers, the double FP can optimized by variation of its friction coefficients μ_1 and μ_2 . In the optimization process μ_1 and μ_2 can take different (and equal) values. Different friction coefficients result in different relative motions on surfaces 1 and 2. Therefore, an articulated slider for the double FP is considered (Fig.1(b)).

2.8 Optimization Procedure

The triple and double FPs are optimized in the following way (Table 1):

- a) The coupled nonlinear equations of motion of the structure with FP (described in section 3) are solved in the time domain.
- b) The El Centro NS, the Kobe, the Loma Prieta and the Northridge accelerograms are adopted for the ground excitation of the isolated structure.

- c) The accelerograms are scaled to the three design values PGA_{opt} at which the FPs are optimized (section 2.2).
- d) The friction coefficients μ_1 and μ_4 of the triple FP and μ_1 and μ_2 of the double FP, respectively, are varied within 0.5% to 25% with increment of 0.5%.
- e) For each PGA_{opt} -scaled earthquake and for each combination of the friction coefficients μ_1 and μ_4 of the triple FP and μ_1 and μ_2 of the double FP, respectively, one full time history analysis of the isolated structure is computed which gives approx. **10800 optimization runs** for the triple FP and the same amount for the double FP.
- f) Each run is evaluated in terms of absolute structural acceleration $max(|\ddot{u}_s + \ddot{u}_g|)$.

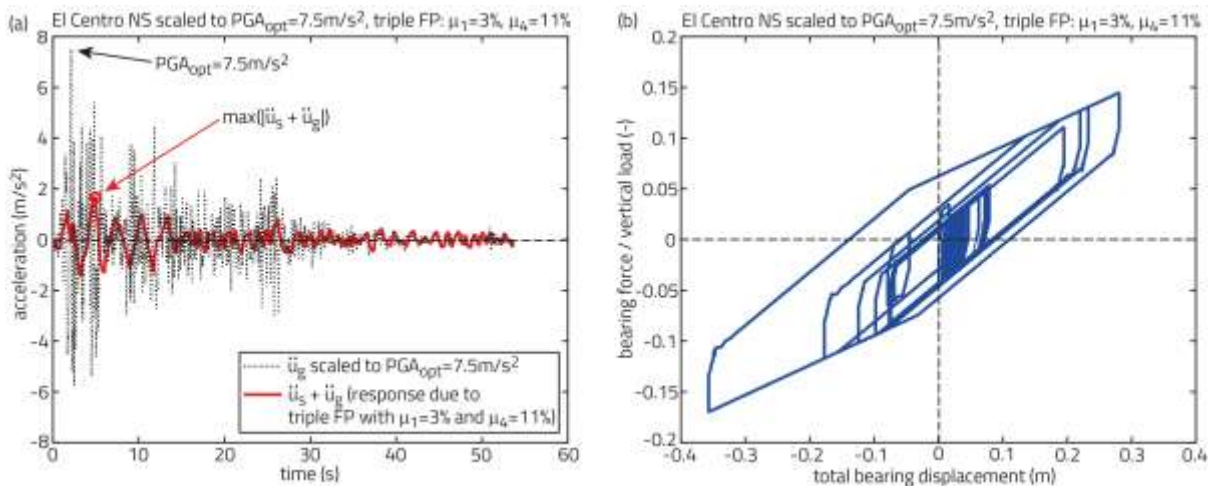


Figure 2. Example of one optimization run for El Centro NS accelerogram scaled to $PGA_{opt}=7.5\text{ m/s}^2$ and triple FP with $\mu_1=3\%$ and $\mu_4=11\%$ triggering sliding regimes I, II and III.

Table 1. Parameters of realistic triple and double FPs for $T_{isolation}=3.5\text{ s}$.

	triple FP	double FP
parameters determined by $T_{isolation}$ and common design approach	$R_{eff-1} = R_{eff-4} = 1.522\text{ m}$ $R_{eff-2} = R_{eff-3} = 0.190\text{ m}$ $\mu_2 = \mu_3 = 1.75\%$ $d_2 = d_3 = 0.07\text{ m}$	$R_{eff-1} = R_{eff-2} = 1.522\text{ m}$
optimization parameters	μ_1 and μ_4	μ_1 and μ_2
variation range	0.5% to 25% with increment of 0.5%	0.5% to 25% with increment of 0.5%
geometrical parameters of realistic FP	$R_1 = R_4 = 1.722\text{ m}$ $R_2 = R_3 = 0.310\text{ m}$ $h_1 = h_4 = 0.20\text{ m}$ $h_2 = h_3 = 0.12\text{ m}$ $d_1 = d_4 = 0.23\text{ m}$ $d_{tot} = 0.60\text{ m}$ $m_4 = 853\text{ kg}$ $m_3 = 258\text{ kg}$ $m_2 = 465\text{ kg (slider)}$	$R_1 = R_2 = 1.722\text{ m}$ $h_1 = h_2 = 0.20\text{ m}$ $d_1 = d_4 = 0.30\text{ m}$ $d_{tot} = 0.60\text{ m}$ $m_2 = 853\text{ kg}$ $m_1 = 465\text{ kg (slider)}$

An example of one optimization run is depicted in Fig. 2. The selected ground acceleration is the accelerogram of the El Centro North-South earthquake that is scaled to $PGA_{opt}=7.5 \text{ m/s}^2$ (Fig. 2(a)). The triple FP is computed for the selected friction coefficients $\mu_1=3\%$ and $\mu_4=11\%$ whereby sliding regimes I (articulated slider assembly), II and III are activated (Fig. 2(b)). The absolute acceleration $\ddot{u}_s(t)+\ddot{u}_g(t)$ of the structure is computed as function of time by solving the coupled nonlinear equations of motion of the structure with triple FP (section 3) in the time domain for the selected ground excitation. Subsequent to each run of one full time history, the absolute maximum $\max(|\ddot{u}_s+\ddot{u}_g|)$ of the absolute structural acceleration is determined by post-processing.

III. MODELLING

3.1 Structure With Triple FP

The structural properties are selected so that the building with base isolation represents a very typical case. The natural frequency f_r of the structure without base isolation is assumed to be 1.2 Hz whereby its natural period of 0.833 s is close to or even within the plateau of the response spectrum. Such a building therefore requires being base isolated. In view of the isolation time period of 3.5 s, which is more than three times longer than the time period of the non-isolated structure, it is common practice to model the isolated building as a single degree-of-freedom system [37]. The according equation of motion of the structure coupled to the bearing plate 4 of the triple FP becomes

$$m_s \ddot{u}_s + c_s (\dot{u}_s - \dot{u}_4) + k_s (u_s - u_4) = -m_s \ddot{u}_g \quad (9)$$

where m_s (=1223.2 metric tonnes), c_s and k_s are the modal mass, the viscous damping coefficient (corresponding to the modal damping ratio $\zeta_s = c_s / (2\sqrt{k_s m_s}) = 1\%$) and the stiffness coefficient of the structure; u_s , \dot{u}_s and \ddot{u}_s are the relative displacement, velocity and acceleration of the structure while u_4 and \dot{u}_4 denote the displacement and velocity of bearing plate 4 of the triple FP relative to the ground. The equation of motion of bearing plate 4 with mass m_4 is

$$m_4 \ddot{u}_4 + f_{h-4} + \frac{W}{R_{eff-4}} (u_4 - u_3) = c_s (\dot{u}_s - \dot{u}_4) + k_s (u_s - u_4) - m_4 \ddot{u}_g \quad (10)$$

where f_{h-4} describes the friction force of sliding surface 4 by the hysteretic friction force model [38]

$$f_{h-4} = \begin{cases} k_h (u_4 - u_3) & : \text{pre-sliding} \\ \mu_4 W \text{sgn}(\dot{u}_4 - \dot{u}_3) & : \text{sliding} \end{cases} \quad (11)$$

where the pre-sliding stiffness coefficient k_h is considered to be two orders of magnitude greater than the stiffness due to the effective radius R_{eff-4} and $W = 12000 \text{ kN}$ denotes the vertical load on the triple FP. u_i , \dot{u}_i and \ddot{u}_i are the relative displacement, velocity and acceleration of plate i (Fig. 1(a)). Since the simulations are made without the consideration of sliding regime V as explained in section 2.5, equation (10) does not include any restrainer force. The equation of motion of sliding plate 3 with mass m_3 becomes

$$m_3 \ddot{u}_3 + f_{h-3} + \frac{W}{R_{eff-3}} (u_3 - u_2) + f_{r-3} = f_{h-4} + \frac{W}{R_{eff-4}} (u_4 - u_3) - m_3 \ddot{u}_g \quad (12)$$

where f_{h-3} is the friction force of sliding surface 3 that is modelled similarly to (11). f_{r-3} describes the force of the restrainer of concave plate 3 that is assumed to be a linear stiffness force if the restrainer is triggered [29]

$$f_{r-3} = \begin{cases} k_r (|u_3 - u_2| - d_3) \text{sgn}(u_3 - u_2) & : |u_3 - u_2| \geq d_3 \\ 0 & : |u_3 - u_2| < d_3 \end{cases} \quad (13)$$

where k_r denotes the restrainer stiffness coefficient that is also assumed to be two orders of magnitude greater than W/R_{eff-4} . The equation of motion of the slider with mass m_2 is

$$m_2 \ddot{u}_2 + f_{h-2} + \frac{W}{R_{eff-2}} (u_2 - u_1) + f_{r-2} = f_{h-3} + \frac{W}{R_{eff-3}} (u_3 - u_2) + f_{r-3} - m_2 \ddot{u}_g \quad (14)$$

where f_{h-2} is the friction force and f_{r-2} the restrainer force of sliding surface 2; both forces are modelled analogically to (11) and (13), respectively. The equation of motion of concave plate 1 with mass m_1

becomes

$$m_1 \ddot{u}_1 + f_{h-1} + \frac{W}{R_{eff-1}} u_1 = f_{h-2} + \frac{W}{R_{eff-2}} (u_2 - u_1) + f_{r-2} - m_1 \ddot{u}_g \quad (15)$$

where the friction force f_{h-1} is a function of u_1 only

$$f_{h-1} = \begin{cases} k_h u_1 & : \text{pre-sliding} \\ \mu_1 W \operatorname{sgn}(\dot{u}_1) & : \text{sliding} \end{cases} \quad (16)$$

As for concave plate 4 also concave plate 1 does not include a restrainer. Hence, there is no restrainer force on the left side of equation (15).

3.2 Structure With Double FP

The modelling of the structure with double friction pendulum is analogue that of the building with triple friction pendulum with the basic difference that only three coupled nonlinear differential equations must be solved due to the mass of the building, the mass of plate 2 of the double FP and the mass of the slider of the double FP.

3.3 Simulation Tool

The coupled nonlinear differential equations of the structure with triple FP and double FP, respectively, are programmed in Matlab/Simulink® environment and solved in the time domain using the solver ode15s(stiff/NDF) with variable step size with upper bound of 0.1 ms and relative tolerance of 1e-3.

IV. OPTIMIZATION RESULTS

Figs. 3 to 5 show how the isolation performances $\max(|\ddot{u}_s + \ddot{u}_g|)$ of the triple and double FPs depend on the selection of their optimization parameters μ_1 and μ_4 and μ_1 and μ_2 , respectively, for the El Centro NS earthquake and for the three selected values of PGA_{opt} at which the optimizations are performed. In order not to overload the paper with too many figures the optimization results for the Kobe, the Loma Prieta and the Northridge earthquakes are only shown for $PGA_{opt}=5.0 \text{ m/s}^2$ (Figs. 6 to 8); the optimization surfaces resulting from $PGA_{opt}=2.5 \text{ m/s}^2$ and $PGA_{opt}=7.5 \text{ m/s}^2$ are similar. The following observations can be made from Figs. 3 to 8:

- The **solution of the optimization problem is “symmetric”** relative to the two optimization parameters, i.e. it is not important which friction coefficient takes which optimal value but only the optimal combination is relevant.
- The **global optimum can be given by a pair of unequal or equal friction coefficients**.
- The optimizations of the triple and double FPs yield similar optimization surfaces (equal scaling on z-axis).
- With increasing PGA_{opt} the optimal friction coefficients become greater because the friction force should be adjusted in proportion to the bearing displacement amplitude as demonstrated in [36, 39]
- **The optimally tuned triple and double FPs yield approx. the same absolute maxima of the absolute structural acceleration (Table 2).** In two cases the isolation performance of the optimal triple FP is more than 5% better than that of the double PF and in two cases the isolation performance of the optimal double FP is more than 5% better than that of the triple PF (17). Thus, the optimized triple and double FPs perform approximately equally well.
- There exists a suboptimal solution with equal friction coefficients that is identical to the optimal solution in some cases. The suboptimally tuned triple and double FPs also evoke approx. the same isolation performances (Table 3).
- The optimization of the triple and double FPs for the Northridge earthquake leads to very small optimal friction coefficients μ_1 and μ_4 and μ_1 and μ_2 , respectively. This is explained by the fact that the friction coefficient should be selected small if the difference between frequency of the isolated structure ($T_{isolation}=3.5 \text{ s}$) and the frequency of the highest energy of the ground acceleration is large [41]: The highest energy density of the El Centro NS earthquake is at 1.47 Hz, of the Kobe earthquake at 0.83 Hz, of the Loma Prieta earthquake at 0.59 Hz and of the Northridge earthquake at 1.76 Hz.

$$\Delta = \frac{\left\{ \max(|\ddot{u}_s + \ddot{u}_g|) \right\}_{triple} - \left\{ \max(|\ddot{u}_s + \ddot{u}_g|) \right\}_{double}}{\left\{ \max(|\ddot{u}_s + \ddot{u}_g|) \right\}_{triple}} \quad (17)$$

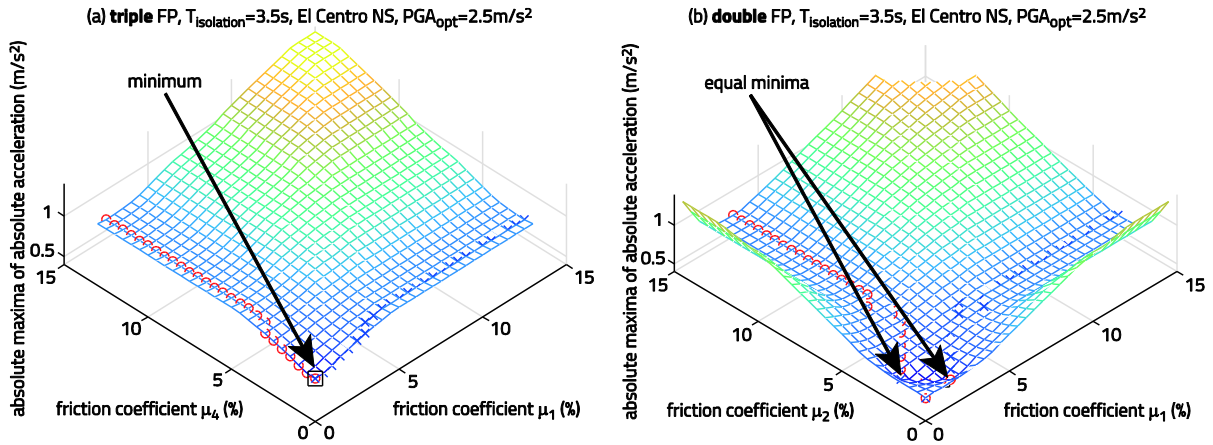


Figure 3. Absolute maxima of absolute structural acceleration due to (a) triple FP and (b) double FP for El Centro NS accelerogram scaled to $PGA_{opt}=2.5 m/s^2$.

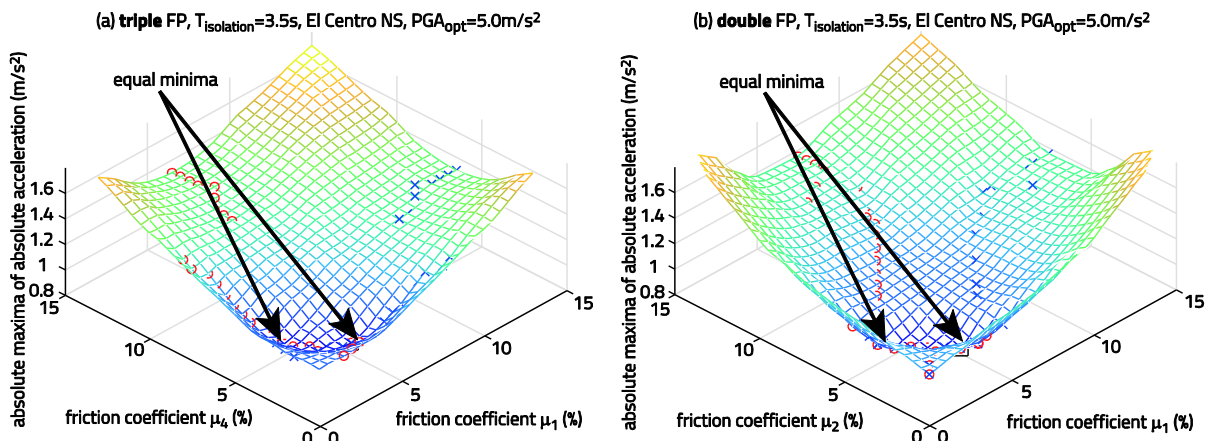


Figure 4. Absolute maxima of absolute structural acceleration due to (a) triple FP and (b) double FP for El Centro NS accelerogram scaled to $PGA_{opt}=5.0 m/s^2$.

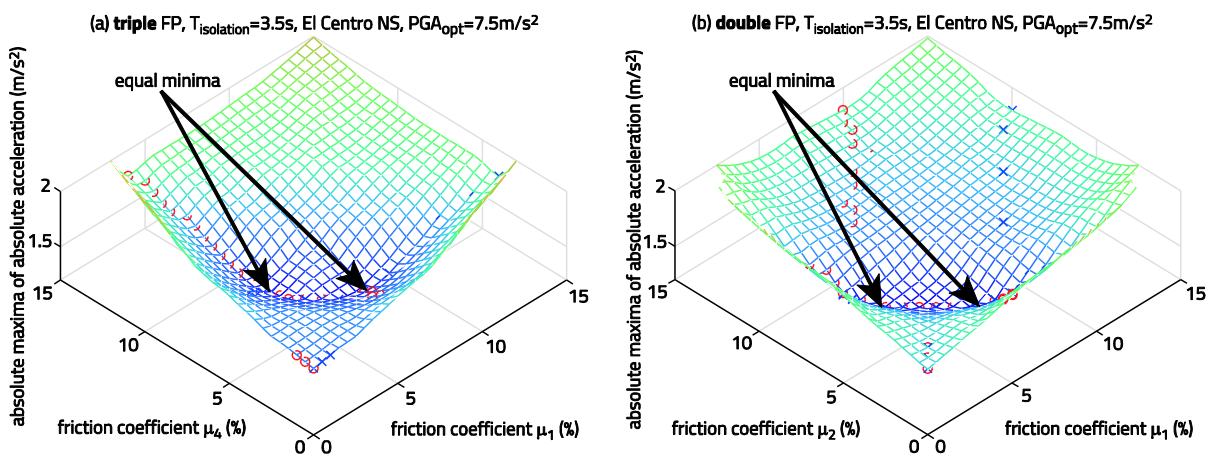


Figure 5. Absolute maxima of absolute structural acceleration due to (a) triple FP and (b) double FP for El Centro NS accelerogram scaled to $PGA_{opt}=7.5 m/s^2$.

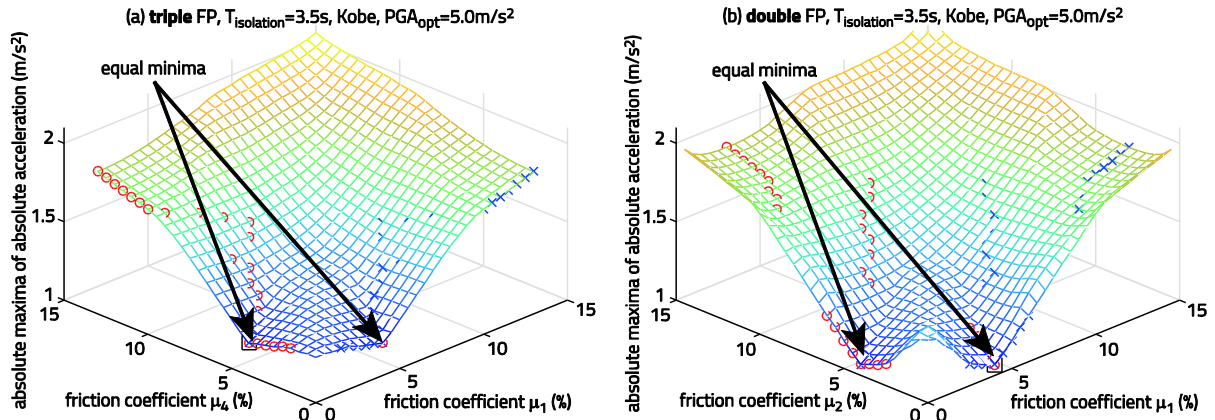


Figure 6. Absolute maxima of absolute structural acceleration due to (a) triple FP and (b) double FP for Kobe accelerogram scaled to $PGA_{opt}=5.0 m/s^2$.

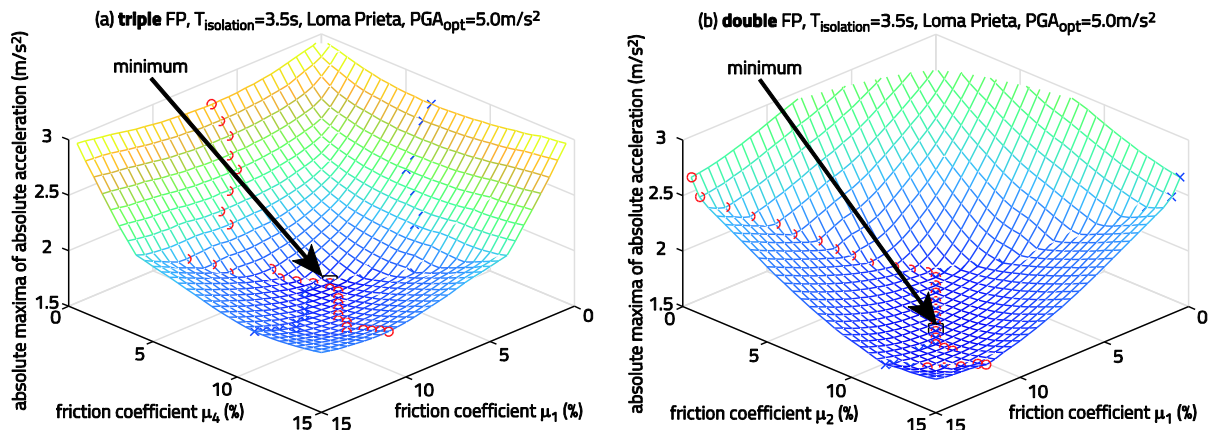


Figure 7. Absolute maxima of absolute structural acceleration due to (a) triple FP and (b) double FP for Loma Prieta accelerogram scaled to $PGA_{opt}=5.0 m/s^2$.

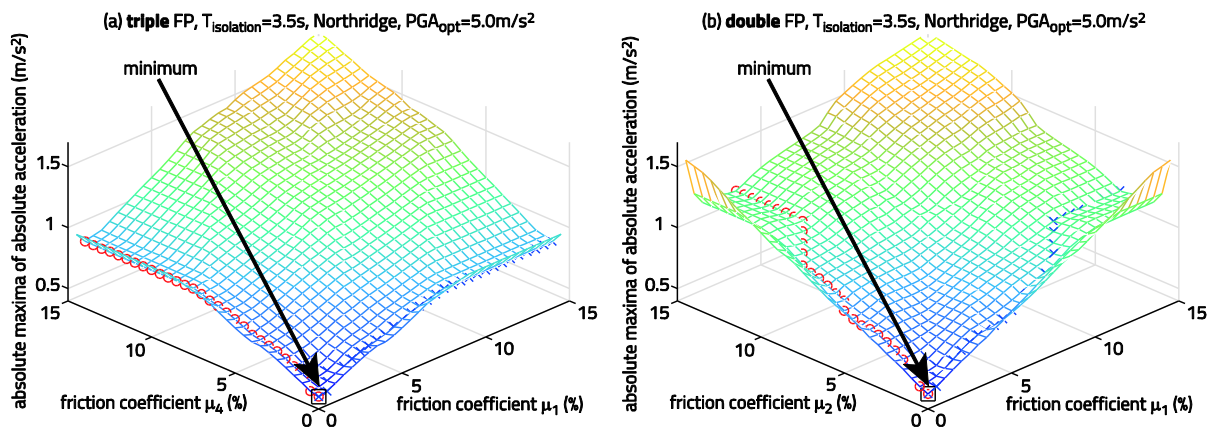


Figure 8. Absolute maxima of absolute structural acceleration due to (a) triple FP and (b) double FP for Northridge accelerogram scaled to $PGA_{opt}=5.0 m/s^2$.

Table 2. Friction coefficients and associated isolation performances of optimal triple FP and optimal double FP.

optimal solution		triple FP			double FP			
accelerogram	PGA (m/s ²)	μ_1 (%)	μ_4 (%)	$\ddot{u}_s + \ddot{u}_g$ (m/s ²)	μ_1 (%)	μ_2 (%)	$\ddot{u}_s + \ddot{u}_g$ (m/s ²)	Δ (-)
El Centro NS	2.5	2.0	2.0	0.416	1.5	2.5	0.423	0.0168
	5.0	3.5	5.5	0.823	3.0	5.0	0.846	0.0279
	7.5	5.5	8.0	1.234	4.5	7.5	1.270	0.0292
Kobe	2.5	2.0	3.5	0.579	0.5	2.5	0.543	-0.0622
	5.0	2.0	6.0	1.032	0.5	4.5	1.025	-0.0068
	7.5	2.0	8.5	1.494	0.5	6.5	1.523	0.0194
Loma Prieta	2.5	4.0	4.0	0.830	5.0	5.0	0.832	0.0024
	5.0	8.0	8.0	1.740	10.5	10.5	1.665	-0.0431
	7.5	12.0	12.0	2.666	16.0	16.0	2.496	-0.0638
Northridge	2.5	0.5	0.5	0.243	0.5	0.5	0.252	0.0370
	5.0	0.5	0.5	0.440	0.5	0.5	0.465	0.0568
	7.5	1.0	1.0	0.649	0.5	1.0	0.700	0.0786

Table 3. Friction coefficients and associated isolation performances of suboptimal ($\mu_1 = \mu_4$) triple FP and suboptimal ($\mu_1 = \mu_2$) double FP (#: identical with optimal solution).

suboptimal solution (equal friction coefficients)		triple FP		double FP	
accelerogram	PGA (m/s ²)	$\mu_1 = \mu_4$ (%)	$\ddot{u}_s + \ddot{u}_g$ (m/s ²)	$\mu_1 = \mu_2$ (%)	$\ddot{u}_s + \ddot{u}_g$ (m/s ²)
El Centro NS	2.5	2.0 [#]	0.416	2.0	0.426
	5.0	4.0	0.834	4.0	0.852
	7.5	6.5	1.262	6.0	1.276
Kobe	2.5	2.0	0.590	1.5	0.612
	5.0	2.0	1.113	3.5	1.222
	7.5	2.5	1.659	4.0	1.834
Loma Prieta	2.5	4.0 [#]	0.830 [#]	5.0 [#]	0.832 [#]
	5.0	8.0 [#]	1.740 [#]	10.5 [#]	1.665 [#]
	7.5	12.0 [#]	2.666 [#]	16.0 [#]	2.496 [#]
Northridge	2.5	0.5 [#]	0.243 [#]	0.5 [#]	0.252 [#]
	5.0	0.5 [#]	0.440 [#]	0.5 [#]	0.465 [#]
	7.5	1.0 [#]	0.649 [#]	1.0	0.725

V. ISOLATION PERFORMANCE ASSESSMENT OF OPTIMIZED TRIPLE FP

Section 4 optimized the triple and double FPs for 12 different DBEs with different frequency contents and different PGAs. The aim of this section is to assess the optimized FPs for the same earthquakes but scaled to different PGAs in order to check if the adaptive behaviour of the triple FP being optimized for the PGA of the DBE leads to a better performance compared to the non-adaptive double FP when other PGAs are considered. The maximum PGA value is set to 150% of PGA_{opt} representing earthquakes in the vicinity of the MCE. In addition to the absolute maxima of the absolute structural acceleration also the absolute maxima of the total bearing displacements are evaluated as the required displacement capacity of FPs is a relevant economical parameter. It is repeated that the structural drifts are not given in this study because if the structure is modelled as a single degree-of-freedom system structural peak accelerations and structural peak drifts are in proportion, see [36].

As hypothetical benchmark a pendulum without friction but with optimal linear viscous damping is also computed because the isolation performance of a linear isolator does not depend on the PGA whereby it yields the optimal solution within the entire PGA range for passive and non-adaptive isolators. The isolation performances and bearing displacements due to the optimal and suboptimal triple and double FPs and for the El Centro NS earthquake are depicted in Figs. 9 to 11. These figures also include the simulation results of the triple FP with $\mu_1=3\%$ and $\mu_4=11\%$ according to the design presented in [30]. For the Kobe, the Loma Prieta and the Northridge earthquakes only the assessment results due to the triple and double FPs optimized at $PGA_{opt}=5.0\text{ m/s}^2$ are depicted in Figs. 12 to 14 in order to limit the number of figures. The inspection of all assessment results plotted in these figures shows:

- For the El Centro NS, the Kobe and the Northridge earthquakes the isolation performances and total bearing displacements due to optimal and suboptimal triple and double FPs are similar within the tested PGA range.

- The results due to the Loma Prieta earthquake show that the optimized triple FP generates a better isolation at $PGA < PGA_{opt}$ while the optimized double FP performs better at $PGA > PGA_{opt}$. This result is caused by the articulated slider assembly with low friction of 1.75% that improves the isolation at $PGA < PGA_{opt}$ for the triple FP while the small friction of the slider assembly is too small to dissipate enough energy at $PGA > PGA_{opt}$ where the double FP with higher friction coefficients (Tables 2 and 3) evokes better isolation results.
- The triple FP designed according to [30] with significantly different friction coefficients μ_1 and μ_4 performs significantly worse than the optimal and suboptimal triple and double FPs.

The comparison with the isolation performance of the pendulum with optimized linear viscous damping reveals:

- Due to the nonlinear behaviours of the triple and double FPs these isolators can only be optimized at one PGA.
- The isolation performances of the triple and double FPs at $PGA = PGA_{opt}$ are slightly worse than that due to optimal linear viscous damping because friction damping introduces higher frequency components into the structure due to the instantaneous working behaviour of friction dampers as explained in [39, 40].
- Optimal linear viscous damping generates PGA-independent isolation of the structure while the isolation performance due friction damping worsens with increasing difference between the PGA value of assessment and the PGA value of optimization.
- The pendulum with optimal linear viscous damping does not only improve the isolation performance of the structure at PGAs considerably smaller and larger than PGA_{opt} compared to both optimized FPs but also results in significantly smaller maximum total bearing displacements.

VI. CONCLUSION

Friction pendulums (FPs) are nonlinear devices due to their energy dissipation by friction damping. As a result, these isolators can only be optimized for maximum isolation of the structure at one PGA value whereby the isolation performance is suboptimal at smaller and larger PGAs. The aim of the triple FP is to improve this drawback of passive FPs by its adaptive behaviour, i.e. stiffness and friction of the triple FP depend on the actual bearing displacement and consequently on the PGA value.

In contrast to previous studies where the isolation performance of triple FPs were computed based on the designs of the friction coefficients, effective radii and displacement capacities of the triple FP as published this paper presents a new approach to assess the isolation performance of the triple FP. First, the triple FP is optimized for minimum absolute structural acceleration, for realistic structural parameters and for the often adopted isolation time period of 3.5 s. The optimization is based on two reasonable assumptions: 1) The design of the articulated slider assembly is in agreement with the available literature and 2) sliding regime V that is not intended to improve the isolation performance but to decrease the maximum bearing displacement capacity due to earthquakes in the vicinity of the MCE is omitted whereby the optimization can be made without the highly nonlinear impacts of restrainers 1 and 4. Due to these assumptions the triple FP can be optimized by variation of the friction coefficients 1 and 4 of the primary sliding surfaces 1 and 4 only whereby the optimization problem becomes numerically manageable. In addition, the optimization results can be plotted as three-dimensional optimization surfaces which show qualitatively and quantitatively the sensitivity of the peak accelerations on the friction tunings. The optimizations are performed for four real earthquakes that are scaled to three PGA values whereby the triple FP is optimized for 12 different DBEs with different frequency contents and PGAs. In a second stage the isolation performances of the optimized triple FPs are computed for the same earthquakes but scaled to various PGAs ranging from very small values up to 150% of the PGA value at which the optimization was made. As benchmark, the isolation performance of the optimized non-adaptive double FP is computed.

The results demonstrate that the optimized triple and double FPs yield approx. the same isolation of the structure at approx. the same total bearing displacement which is explained by the observation that the optimal solutions of the triple FP and double FP are very similar.

ACKNOWLEDGEMENT

The authors gratefully acknowledge the financial support of MAURER SE, Munich, Germany.

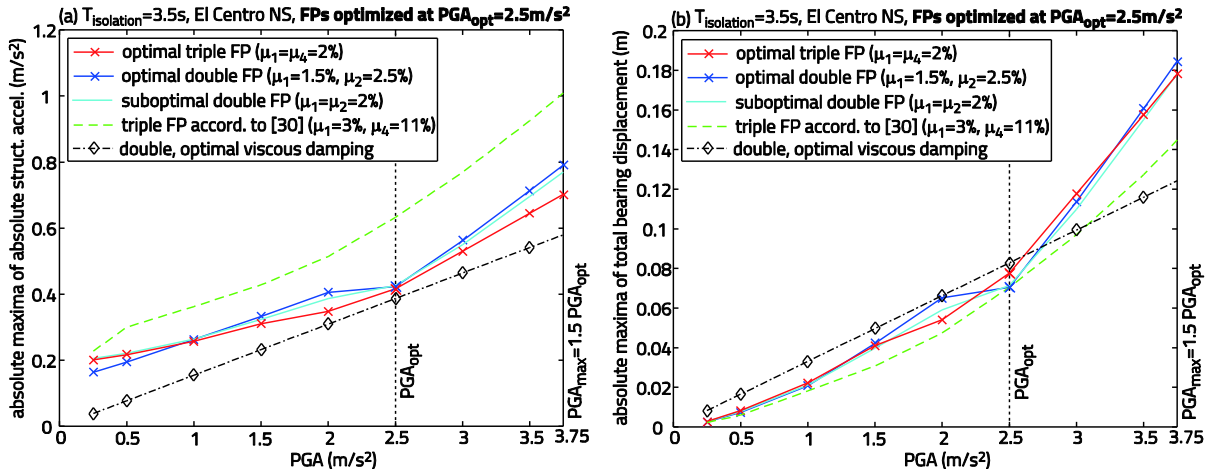


Figure 9. Performance assessment of triple and double FPs optimized for El Centro NS accelerogram scaled to $PGA_{opt}=2.5\text{ m/s}^2$.

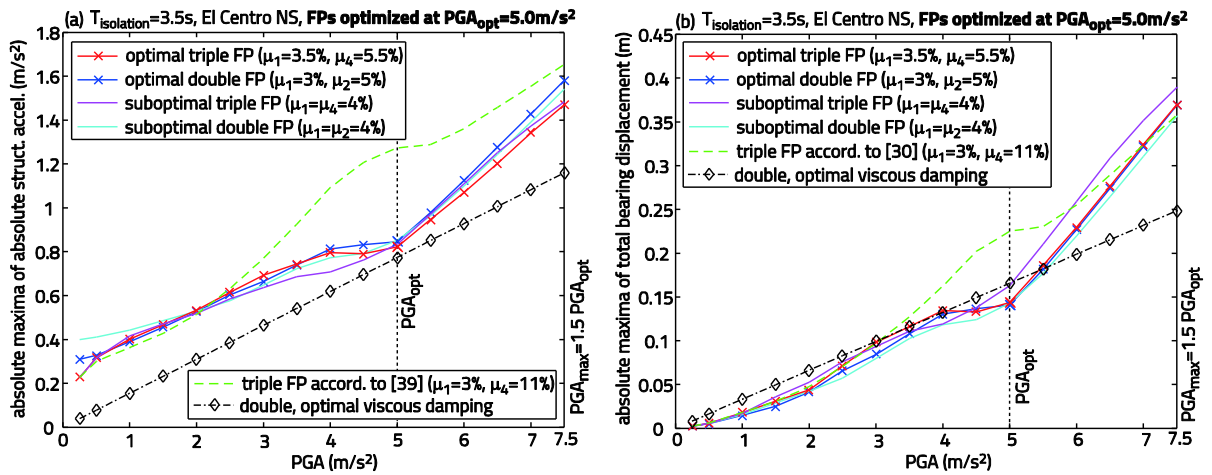


Figure 10. Performance assessment of triple and double FPs optimized for El Centro NS accelerogram scaled to $PGA_{opt}=5.0\text{ m/s}^2$.

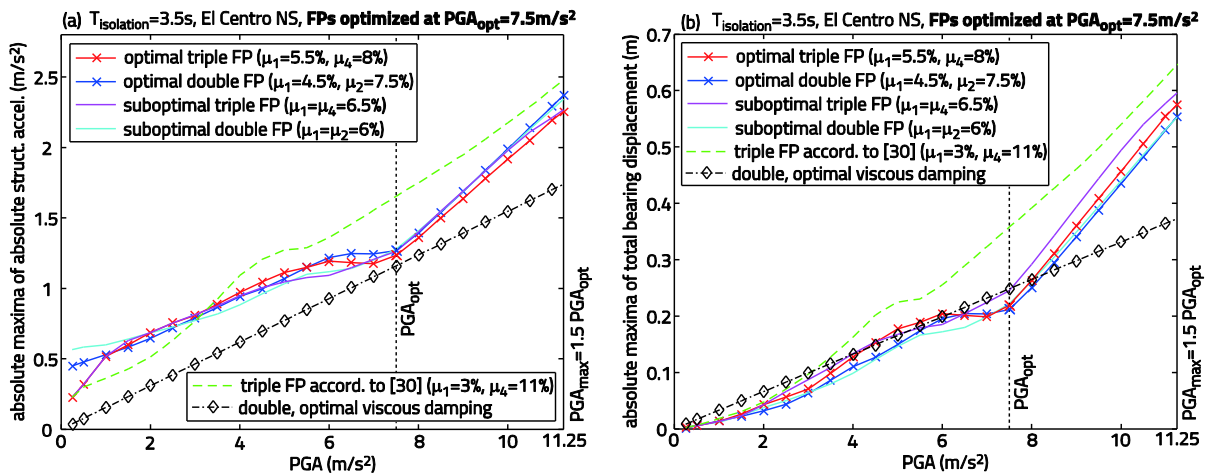


Figure 11. Performance assessment of triple and double FPs optimized for El Centro NS accelerogram scaled to $PGA_{opt}=7.5\text{ m/s}^2$.

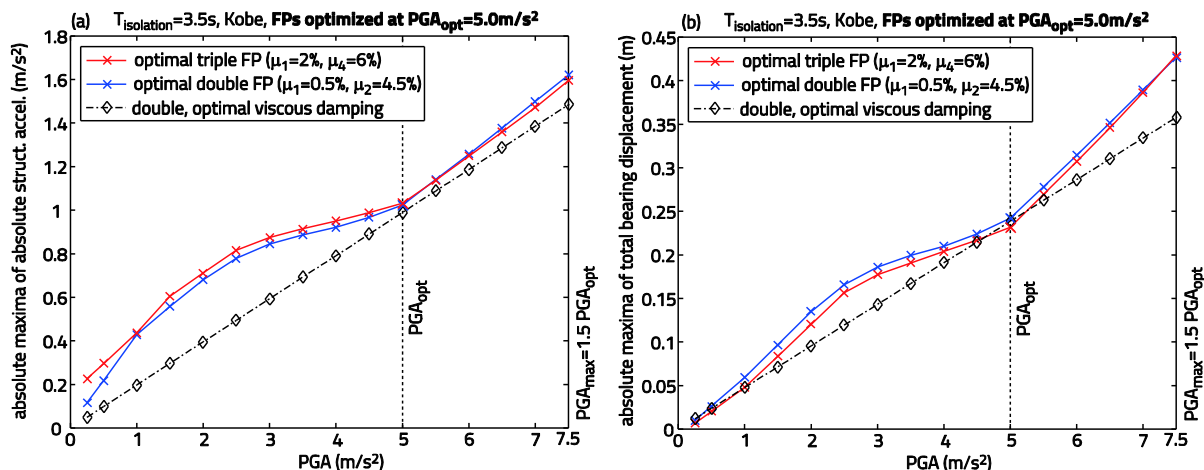


Figure 12. Performance assessment of triple and double FPs optimized for Kobe accelerogram scaled to $PGA_{opt} = 5.0 m/s^2$.

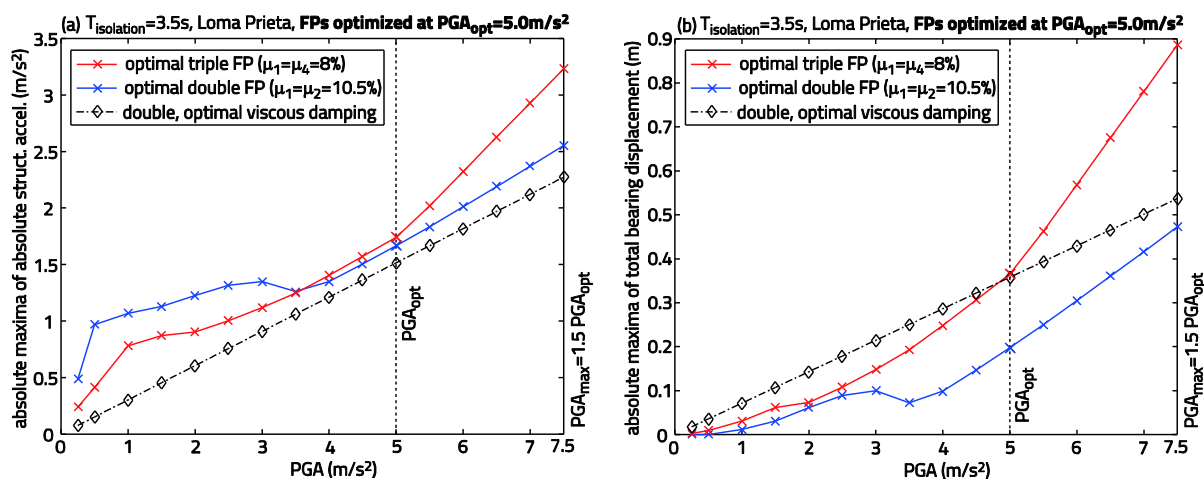


Figure 13. Performance assessment of triple and double FPs optimized for Loma Prieta accelerogram scaled to $PGA_{opt} = 5.0 m/s^2$.

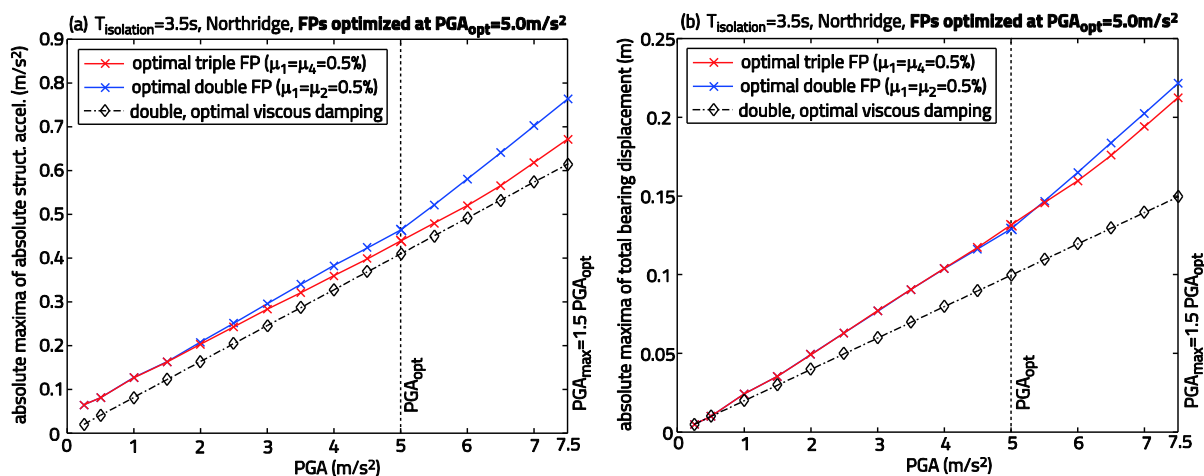


Figure 14. Performance assessment of triple and double FPs optimized for Northridge accelerogram scaled to $PGA_{opt} = 5.0 m/s^2$.

REFERENCES

- [1]. R.I. Skinner, W.H. Robinson, and G.H. McVerry, An introduction to seismic isolation (Wiley: Chichester, England, 1993).
- [2]. A.K. Chopra, Dynamics of Structures: Theory and Applications to Earthquake Engineering (Prentice-Hall, 1995).
- [3]. F. Naeim, and J.M. Kelly, Design of Seismic Isolated Structures (Wiley: New York, 1999).
- [4]. C.A. Cornell, Engineering Seismic Risk Analysis, Bulletin of the Seismological Society of America, 58, 1968, 1583-1606.
- [5]. M. Imbimbo, and J.M. Kelly, Stability aspects of elastomeric isolators, Earthquake Spectra, 13(3), 1997, 431-449.
- [6]. V.A. Zayas, S.S. Low, and S.A. Mahin, The FPS earthquake resisting system experimental report, Technical Report UBC/EERC-87/01, 1987.
- [7]. T.M. Al-Hussaini, V.A. Zayas, and M.C. Constantinou, Seismic isolation of multi-story frame structures using spherical sliding isolation systems, Technical Report NCEER-94-0007, 1994.
- [8]. C.S. Tsai, Finite element formulations for friction pendulum seismic isolation bearings, International Journal for Numerical Methods in Engineering, 40, 1997, 29-49.
- [9]. K.Z.Y. Yen, and Y.J. Lee, Passive vibration isolating system (US Patent No. 6126136, October 3, 2000).
- [10]. Fenz, and M.C. Constantinou, Behaviour of the double concave Friction Pendulum bearing, Earthquake Engng. Struct. Dyn., 35, 2006, 1403-1424.
- [11]. C.S. Tsai, W.-S. Chen, T.-C. Chiang, and B.-J. Chen, Component and shaking table tests for full-scale multiple friction pendulum system, Earthquake Engng. Struct. Dyn., 35, 2006, 1653-1675.
- [12]. C. Bucher, Probability-based optimization of friction damping devices, Structural Safety, 31, 2009, 500-507.
- [13]. R. Medeot, Experimental validation of re-centering capability evaluation based on energy concepts, Proc. 14th World Conference on Earthquake Engineering, October 12-17, 2008, Beijing, China.
- [14]. J.M. Kelly, The role of damping in seismic isolation, Earthquake Engng. Struct. Dyn., 28(1), 1999, 3-20.
- [15]. J.F. Hall, Discussion of 'The role of damping in seismic isolation', Earthquake Engng. Struct. Dyn., 28(12), 1999, 1717-1720.
- [16]. Eurocode 8, Design of structures for earthquake resistance – Part 1: General rules, seismic actions and rules for buildings (EN 1998-1:2004 + AC:2009).
- [17]. M.Q. Feng, M. Shinozuka, and S. Fujii, Friction-controllable sliding isolation system, Journal of Engineering Mechanics (ASCE), 119(9), 1993, 1845-1864.
- [18]. N. Wongprasert, and M.D. Symans, Experimental evaluation of adaptive elastomeric base-isolated structures using variable-orifice fluid dampers, Journal of Structural Engineering (ASCE), 131(6), 2005, 867-877.
- [19]. T. Kobori, M. Takahashi, T. Nasu, and N. Niwa, Seismic response controlled structure with active variable stiffness system, Earthquake Engng. Struct. Dyn., 22, 1993, 925-941.
- [20]. S. Nagarajaiah, and S. Sahasrabudhe, Seismic response control of smart sliding isolated buildings using variable stiffness systems: An experimental and numerical study, Earthquake Engng. Struct. Dyn., 35(2), 2006, 177-197.
- [21]. F. Casciati, L. Faravelli, and K. Hamdaoui, Performance of a base isolator with shape memory alloy bars, Earthquake Engineering and Engineering Vibration, 6(4), 2007, 401-408.
- [22]. N. Makris, Rigidity–plasticity–viscosity: Can electrorheological dampers protect base isolated structures from near-source ground motions?, Earthquake Engng. Struct. Dyn., 26(5), 1997, 571-591.
- [23]. J.C. Ramallo, E.A. Johnson, and B.F. Spencer Jr, 'Smart' base isolation systems, Journal of Engineering Mechanics (ASCE), 128(10), 2002, 1088-1100.
- [24]. P.Y. Lin, P.N. Roschke, C.H. Loh, and C.P. Cheng, Semi-active controlled base-isolation system with magnetorheological damper and pendulum system, Proceedings of the 13th World Conference on Earthquake Engineering, Vancouver, BC, Canada, 2004; Paper 691.
- [25]. H. Li, and J. Ou, A design approach for semi-active and smart base-isolated buildings, Structural Control and Health Monitoring, 13(2-3), 2006, 660-681.
- [26]. F. Weber, and M. Mašlanka, Precise Stiffness and Damping Emulation with MR Dampers and its Application to Semi-active Tuned Mass Dampers of Wolgograd Bridge, Smart Mater. Struct., 23, 2014, 015019.
- [27]. F. Weber, Robust force tracking control scheme for MR dampers, Struct. Control Health Monit., 22(12), 2015, 1373-1395.

- [28]. A. Pocanschi, and M.C. Phocas, Earthquake isolator with progressive nonlinear deformability, *Engineering Structures*, 29, 2007, 2586-2592.
- [29]. D.M. Fenz, and M.C. Constantinou, Spherical sliding isolation bearings with adaptive behavior: Theory, *Earthquake Engng. Struct. Dyn.*, 37, 2008, 163-183.
- [30]. D.M. Fenz, and M.C. Constantinou, Spherical sliding isolation bearings with adaptive behavior: Experimental verification, *Earthquake Engng. Struct. Dyn.*, 37, 2008, 185-205.
- [31]. D.M. Fenz, and M.C. Constantinou, Modeling Triple Friction Pendulum Bearings for Response-History Analysis, *Earthquake Spectra*, 24(4), 2008, 1011-1028.
- [32]. F. Fadi, and M.C. Constantinou, Evaluation of simplified methods of analysis for structures with triple friction pendulum isolators, *Earthquake Engng. Struct. Dyn.*, 39, 2010, 5-22.
- [33]. N.D. Dao, K.L. Ryan, E. Sato, and T. Sasaki, Predicting the displacement of Triple Pendulum bearings in a full scale shaking experiment using a three-dimensional element, *Earthquake Engng. Struct. Dyn.*, 42, 2013, 1677-1695.
- [34]. A.P. Giammona, K.L. Ryan, and N.D. Dao, Evaluation of Assumptions Used in Engineering Practice to Model Buildings Isolated with Triple Pendulum Isolators in SAP2000, *Earthquake Spectra*, 31(2), , 637-660.
- [35]. C. Bucher, Analysis and Design of Sliding Isolation Pendulum Systems, Proc. IABSE Conference Nara, May 13-15, 2015.
- [36]. F. Weber, H. Distl, and C. Braun, Dynamic Characterization and Isolation Performance of Triple Friction Pendulum, Proceedings of the 8th World Congress on Joints, Bearings and Seismic Systems for Concrete Structures (IJBRC), Atlanta, Georgia, USA, September 25-29, 2016.
- [37]. C.S. Tsai, T.-C. Chiang, and B.-J. Chen, Experimental evaluation of piecewise exact solution for predicting seismic responses of spherical sliding type isolated structures, *Earthquake Engng. Struct. Dyn.*, 34, 2005, 1027-1046.
- [38]. F. Al-Bender, V. Vincent Lampaert, and J. Swevers, The Generalized Maxwell-Slip Model: A Novel Model for Friction Simulation and Compensation, *IEEE Transactions on Automatic Control*, 50(11), 2005, 1883-1887.
- [39]. F. Weber, and C. Boston, Energy Based Optimization of Viscous-Friction Dampers on Cables, *Smart Mater. Struct.*, 19, 2010, 045025 (11pp).
- [40]. F. Weber, J. Høgsberg, and S. Krenk, Optimal tuning of amplitude proportional Coulomb friction damper for maximum cable damping, *Journal of Structural Engineering*, 136(2), 2010, 123-134.
- [41]. A. Preumont, *Vibration Control of Active Structures* (Kluwer Academic Publishers, Dordrecht, 2002).